Journal of Orthopaedic Translation 42 (2023) 15–30

Contents lists available at ScienceDirect

Journal of Orthopaedic Translation

journal homepage: www.journals.elsevier.com/journal-of-orthopaedic-translation

Original Article

Kartogenin-enhanced dynamic hydrogel ameliorates intervertebral disc degeneration via restoration of local redox homeostasis

Xin Tian [a,b,1], Yijian Zhang [a,b,1], Lei Shen [c,1], Guoqing Pan [d], Huilin Yang [a,b], Zhenhuan Jiang [c,*], Xuesong Zhu [a,b,**], Fan He [a,b,***]

[a] Department of Orthopaedics, The First Affiliated Hospital of Soochow University, Soochow University, Suzhou, 215006, China
[b] Orthopaedic Institute, Medical College, Soochow University, Suzhou, 215000, China
[c] Department of Orthopaedics, The Affiliated Yixing Hospital of Jiangsu University, Yixing City, 214200, China
[d] Institute for Advanced Materials, School of Materials Science and Engineering, Jiangsu University, Zhenjiang, 212013, China

ARTICLE INFO

Keywords:
Intervertebral disc degeneration
Nucleus pulposus
Kartogenin
NRF2
Dynamic hydrogel

ABSTRACT

Introduction: Over-activation of oxidative stress due to impaired antioxidant functions in nucleus pulpous (NP) has been identified as a key factor contributing to intervertebral disc degeneration (IVDD). While Kartogenin (KGN) has previously demonstrated antioxidant properties on articular cartilage against osteoarthritis, its effects on NP degeneration have yet to be fully understood.

Objectives: This study aimed to investigate the protective effects of KGN on nucleus pulpous cells (NPCs) against an inflammatory environment induced by interleukin (IL)-1β, as well as to explore the therapeutic potential of KGN-enhanced dynamic hydrogel in preventing IVDD.

Methods: NPCs were isolated from rat caudal IVDs and subjected to treatment with KGN at varying concentrations (ranging from 0.01 to 1 μM) in the presence of IL-1β. The expression of extracellular matrix (ECM) anabolism markers was quantitatively assessed at both the mRNA and protein levels. Additionally, intracellular reactive oxygen species and antioxidant enzyme expression were evaluated, along with the role of nuclear factor erythroid 2-related factor 2 (NRF2). Based on these findings, a dynamic self-healing hydrogel loaded with KGN was developed through interconnecting networks. Subsequently, KGN-enhanced dynamic hydrogel was administered into rat caudal IVDs that had undergone puncture injury, followed by radiographic analysis and immunohistochemical staining to evaluate the therapeutic efficacy.

Results: In vitro treatments utilizing KGN were observed to maintain ECM synthesis and inhibit catabolic activities in IL-1β-stimulated NPCs. The mechanism behind this protective effect of KGN on NPCs was found to involve the asctivation of NRF2 and downstream antioxidant enzymes, including glutathione peroxidase 1 and heme oxygenase 1. This was further supported by the loss of both antioxidant and anabolic effects upon pharmacological inhibition of NRF2. Furthermore, a self-healing hydrogel was developed and loaded with KGN to achieve localized and sustained release of the compound. The injection of KGN-enhanced hydrogel effectively ameliorated the degradation of NP ECM and mitigated inflammation in a rat model of puncture-induced IVDD.

Conclusions: Our results indicate that KGN exhibits potential as a therapeutic agent for NP degeneration, and that KGN-enhanced dynamic hydrogel represents a novel approach for treating IVDD by restoring redox homeostasis in NP.

The translational potential of this article: The dysregulation of oxidant and antioxidant balance has been shown to impede the repair and regeneration of NP, thereby hastening the progression of IVDD following injury. The

* Corresponding author. Department of Orthopaedics, The Affiliated Yixing Hospital of Jiangsu University, No. 75 Tongzhenguan Road, Yixing City, 214200, Jiangsu, China.
** Corresponding author. Department of Orthopaedics, The First Affiliated Hospital of Soochow University, No. 899 Pinghai Road, Suzhou, 215006, Jiangsu, China.
*** Corresponding author. Orthopaedic Institute, Medical College, Soochow University, No. 178 East Ganjiang Road, Suzhou, 215000, Jiangsu, China.
E-mail addresses: jiangzh1018@126.com (Z. Jiang), zhuxs@suda.edu.cn (X. Zhu), fanhe@suda.edu.cn (F. He).
[1] Xin Tian, Yijian Zhang, and Lei Shen contributed equally to this work.

https://doi.org/10.1016/j.jot.2023.07.002
Received 7 February 2023; Received in revised form 29 June 2023; Accepted 6 July 2023

present investigation has demonstrated that the sustained release of KGN promotes the synthesis of ECM in vitro and mitigates the progression of IVDD in vivo by restoring redox equilibrium, thereby presenting a novel therapeutic candidate based on the antioxidant properties of KGN for the treatment of IVDD.

1. Introduction

Over the past three decades, low back pain (LBP) has emerged as the primary cause of lived with disability years (YLDs) on a global scale [1]. Intervertebral disc degeneration (IVDD), a prevalent spinal condition characterized by the deterioration of one or more discs, is frequently associated with LBP, affecting nearly 50% of individuals [2]. Current clinical interventions for IVDD involve conservative analgesia medication or intervertebral disc (IVD) fusion procedures, yet the effectiveness of these strategies remains suboptimal [3]. Under physiological conditions, the nucleus pulposus (NP) is characterized by a high concentration of collagen, proteoglycan, and water, which collectively confer exceptional biological and mechanical properties to the IVD [4]. However, pathological stimuli such as aging, infection, physical activity, or injury can disrupt the extracellular matrix (ECM) metabolism in the NP tissue [5], leading to an imbalance between matrix synthesis and degradation, and an overactivation of catabolic enzymes [6].

The modified microenvironment subsequent to NP injury poses a deleterious effect on cellular proliferation, migration, and differentiation, attributable to the inflammatory cascade and cytokine storm [7]. Pro-inflammatory cytokines, such as interleukin-1β (IL-1β) and tumor necrosis factor (TNF)-α, assume a crucial role in the progression of IVDD [8]. These cytokines not only instigate the degradation of IVD matrix but also trigger oxidative stress, culminating in the degeneration of IVD tissues. The introduction of IL-1β into the lumbar IVD of rats elicited a rapid inflammatory response and severe NP herniation [9]. Therefore, the reconstruction of the ECM microenvironment in the IVD is a crucial step in reversing the degeneration process and promoting NP regeneration.

The redox balance plays an indispensable role in cellular activity and is of significant importance to NP metabolism. The degenerative NP presents an overproduction of reactive oxygen species (ROS), including superoxide, hydrogen peroxide (H_2O_2), hydroxyl radical, hydroxyl ion, and nitric oxide (NO) [10], which subsequently induce matrix degradation and compromise the integrity of IVD matrix [11]. A noteworthy association was detected between the levels of ROS and the severity of LBP in patients with IVDD, as evidenced by the analysis of IVD samples [12]. In a similar vein, ROS-targeted therapy has been shown to mitigate IVDD by augmenting anabolism and suppressing pyroptosis mediated by nod-like receptor family pyrin domain protein 3 (NLRP3) [13]. Conversely, a disrupted microenvironment in IVDD is accompanied by an impaired intracellular antioxidant system, which comprises multiple antioxidative enzymes [14]. Nanoparticles that mimic antioxidant enzymes have been shown to rescue IVDD by safeguarding superoxide dismutase 1 (SOD1) from degradation mediated by ubiquitination-proteasome [15]. Consequently, there is a pressing need for biomimetic agents that can regulate redox functions and enhance ECM simultaneously, in order to achieve superior IVDD repair.

The small heterocyclic molecule Kartogenin (KGN) was initially identified as a promoter of chondrogenic differentiation in mesenchymal stem cells (MSCs) by facilitating the nuclear localization of core-binding factor beta subunit (CBF-β) [16]. KGN has been shown to activate the family of small mother against decapentaplegic (SMAD) 4/5 that is commonly associated with various cartilage or bone-related diseases [17]. Shi et al. demonstrated that a rapid ultraviolet-crosslinked scaffold containing KGN effectively recruited endogenous stem cells to facilitate the regeneration of natural hyaline cartilage [18]. A study conducted in our laboratory previously demonstrated that KGN effectively prevented articular cartilage erosion in post-traumatic osteoarthritis (OA) mice by inhibiting the expression of matrix degradation enzymes [19]. Given the similarities in the ECM components of cartilage and NP, KGN has been increasingly utilized for the treatment of IVDD in recent years. The sustained release of KGN from a conjugated chitosan-hyaluronic acid (HA) hydrogel has been shown to enhance the differentiation of adipose-derived stem cells (ADSC) towards NP cells (NPCs) [20]. In the context of simulated degeneration induced by IL-1β or TNF-α, KGN has been observed to induce ECM synthesis in both human NPCs and mice IVD tissues [21]. Despite these findings, the precise role of KGN in modulating NP regeneration and the underlying mechanism remain unclear.

Biomimetic hydrogels have been developed to mimic the microenvironment necessary for cell differentiation, and hold promise for use in tissue engineering [22]. Furthermore, hydrogel-based drug delivery strategies offer a means of achieving localized and sustained release of therapeutic agents [23]. Due to the unique mechanical properties of the ECM in native tissue, conventional hydrogels are susceptible to fragmentation under compression, tensile, or shear forces upon *in vivo* implantation. To overcome this challenge, dynamic hydrogels with an intrinsic reversibly network have been developed, which possess exceptional self-healing capabilities to withstand external mechanical stimuli [24]. In this regard, our recently developed receptor-ligand recognized hydrogel has been designed to mimic the three-dimensional (3D) ECM intelligently, regulating cellular behavior in a dynamic and remoldable manner [25]. Chen et al. developed an injectable and self-healing hydrogel composed of aldehyde hyaluronic acid (HA-CHO) and poly (amidoamine) PAMAM, loaded with small interfering RNA (siRNA), to delay the progression of IVDD by silencing endogenous stimulator of interferon genes (STING) [26]. The hydrogel was characterized as possessing anabolic and antioxidant properties, which effectively prevented damage or degeneration of the IVD ECM.

In this study, we intended to investigated the role of KGN in maintaining ECM equilibrium during IVDD development, and explored the involvement of redox balance in KGN-induced defense against IVDD and the underlying molecular mechanisms. Inspired by the biomimetic microenvironment of NP tissue, a KGN-loaded self-healing hydrogel rendered with local oxidative modulation was prepared. Ultimately, KGN-loaded hydrogel was injected *in situ* to delay the degenerative progression and even promote NP regeneration in puncture-induced IVDD model [27].

2. Material and methods

2.1. NPC isolation and cell culture

NP tissues were harvested from the caudal disc of 6-week-old male Sprague–Dawley (SD) rats. NPCs were then isolated by incubation with 0.2% type II collagenase (Sigma–Aldrich, St. Louis, MO, USA) at 37 °C for 1 h, and the excess tissue fragments were subsequently filtered using a sterile 70-μm cell filter. The NPCs were cultured in Dulbecco's modified Eagle medium (DMEM) supplemented with 10% fetal bovine serum (FBS), 100 units/mL penicillin, and 100 mg/mL streptomycin (all from Thermo Fisher Scientific, Waltham, MA, USA), with the culture medium being replaced every three days. The NPCs at Passage One were utilized for the subsequent experiments.

2.2. In vitro treatment with KGN or inhibitor

A stock solution of 20 mM KGN (Sigma–Aldrich) was prepared by dissolving it in dimethyl sulfoxide (DMSO, Sigma–Aldrich) and subsequently diluted with PBS. The cells were exposed to varying concentrations of KGN (0.01, 0.1, and 1 μM), while the control (CTRL) group

received treatment with 0.005% DMSO. Additionally, NPCs were subjected to treatment with 5 ng/mL recombinant human IL-1β (Thermo Fisher Scientific), followed by KGN administration. To investigate the impact of NRF2 on NP metabolism, cells were pre-treated with 5 μM ML385, a chemical inhibitor of NRF2, and subsequently exposed to 5 ng/mL IL-1β and 1 μM KGN.

2.3. Cell proliferation

Cell viability was assessed through the utilization of the cell counting kit-8 (CCK-8, Beyotime, Haimen, China). Specifically, cells were seeded into 96-well plates at a density of 1000 cells per well and subsequently incubated with a 10% CCK-8 solution at 37 °C for 1 h on days 1, 3, 5, and 7. The optical density (OD) at 450 nm was then measured utilizing a spectrophotometer (BioTek, Winooski, VT, USA).

2.4. Immunofluorescence staining

The cells were subjected to fixation in 4% formaldehyde at room temperature for 30 min, followed by permeation with 0.3% Triton-X 100. Subsequently, the cells were treated with a blocking solution consisting of 5% bovine serum albumin (BSA, Beyotime) for 30 min, and then incubated overnight at 4 °C with anti-COLII antibody (Abcam, Waltham, MA, USA). On the following day, the cells were washed with phosphate buffered saline (PBS) and incubated with a fluorescent secondary antibody for 2 h at room temperature. The resulting images were captured and analyzed semi-quantitatively using Image J software (National Institutes of Health, Bethesda, MD, USA).

2.5. Quantitative reverse transcription-polymerase chain reaction (RT-PCR)

Total RNA was extracted from NPCs using TRIzol (Thermo Fisher Scientific), followed by cDNA synthesis using the RevertAid First-strand cDNA Synthesis Kit (Thermo Fisher Scientific) with 1 μg of RNA. Amplification of cDNA was performed using the iTap Universal SYBR Green Supermix kit (Bio-Rad, Hercules, CA, USA) and the CFX96 Real-Time PCR system (Bio-RAD). The transcription levels of *Col2a1*, *Acan*, *Mmp13*, *Adamts5*, *Nrf2*, heme oxygenase 1 (*Hmox1*), and glutathione peroxidase 1 (*Gpx1*) were determined with glyceraldehyde-3-phosphate dehydrogenase (*Gapdh*) as the standard control. The primer sequences are provided in Supplementary Table 1.

2.6. Western blot

Proteins were extracted from cells through employment of RIPA lysis buffer (Beyotime), which was supplemented with protease inhibitors and phosphatase inhibitors (Thermo Fisher Scientific). The protein concentration was determined via utilization of the BCA protein quantification kit (Beyotime). Subsequently, the proteins were separated through 10% sodium dodecyl sulfate-polyacrylamide gel (SDS-PAGE) electrophoresis and transferred onto PVDF membranes (Beyotime). The membranes were then blocked with QuickBlock blocking buffers (Beyotime) and incubated overnight with primary antibodies, namely anti-COLII (ab188570, Abcam), anti-ACAN (A11691, Abclonal, Wuhan, China), anti-SOX9 (A2479, Abclonal), anti-MMP13 (A11755, Abclonal), anti-ADAMTS5 (A23125, Abclonal), anti-NRF2 (A21176, Abclonal), anti–HO–1 (A1346, Abclonal), and anti-GPX1 (A11166, Abclonal) and α-tubulin (AF0001, Beyotime). Following this, the membranes were incubated with secondary antibody at room temperature. The visualization of protein bands was accomplished through the utilization of a chemiluminescent solution (Thermo Fisher Scientific) and subsequent quantification was conducted via Image J software.

2.7. Synthesis of Gel-SH

One gram of gelatin (Sigma–Aldrich) was dissolved in PBS (pH = 8.0), and then mixed with 32 mg of Traut's Reagent (J&K Scientific, San Jose, CA, USA) at room temperature for 4 h with magnetic stirring. Following this, dialysis was performed using a dialysis bag (MW cutoff = 3000 Da) for 7 d, and the resulting product was freeze-dried for preservation.

2.8. Fabrication of Au-Gel-β-CD hydrogel

A solution of 200 mg Gel-SH in 1.3 mL of PBS was combined with 50 mg of S-β-CD (Macklin, Shanghai, China) with a magnetic stirrer. Subsequently, 7 mg of $HAuCl_4$ (J&K Scientific LLC., San Jose, CA, USA) in 350 μL of PBS was added dropwise to make mercaptocyclodextrin gelatin (Gel-β-CD) hydrogel.

2.9. Encapsulation of KGN

A solution containing 15 mg of KGN in 50 μL DMSO was introduced into the Gel-β-CD solution, followed by the gradual addition of $HAuCl_4$ with stirring to achieve a final concentration of 0.75% KGN in the hydrogel.

2.10. Characterization of KGN-enhanced dynamic hydrogel

2.10.1. Scanning electron microscope (SEM)

In order to examine the microstructure of the hydrogel, dynamic hydrogel samples were subjected to freezing and lyophilization at −80 °C, with and without KGN. These samples were then affixed to an aluminum column, coated with gold via sputtering, and analyzed using a SEM (JSM-7100F, JEOL, Tokyo, Japan) at an accelerated voltage of 15 kV.

2.10.2. Injectable and self-healing properties of dynamic hydrogel

To assess the hydrogel's injectable capacity, it was loaded into a syringe and dispensed through a 22 G needle (KDL, Shanghai, China). The self-healing properties of the hydrogel were evaluated by placing it into two square molds that had been dyed blue or orange, cutting and splicing them together, and incubating the resulting structure in a 37 °C environment for 10 min.

2.10.3. Rheological property of dynamic hydrogel

The rheological measurements of the hydrogel's mechanical properties were conducted using a rheometer AR2000Ex (TA Instruments) on a parallel plate (40 mm Peltier plate Steel). The shear storage modulus (G′) and shear loss modulus (G″) were determined under constant deformation (1%) and temperature (37 °C). The investigation of the hydrogel's self-healing properties involved analyzing the changes in G′ and G″ under alternating oscillating strains of 1% and 300% (low strain 1%, 60 s, high strain 300%, 60 s). The injectability of the hydrogel was assessed through the measurement of shear viscosity under a frequency sweep mode, with shear rates spanning from 0.1 to 50 rad/s.

2.11. Release profile

To assess the *in vitro* sustained release of KGN, hydrogel specimens were subjected to immersion in deionized water at 4 °C for 30 d. The supernatant was subsequently substituted with PBS at predetermined intervals, and the concentration of KGN released from the hydrogels was quantified using a Nanodrop 2000 spectrometer (Thermo Fisher Scientific) at a wavelength of 280 nm.

2.12. Cell viability assay

Cell viability was evaluated using a Live/Dead staining kit (Thermo Fisher Scientific) following the manufacturer's instructions. NPCs were seeded at a density of 12,000 cells per well in 24-well plates and cultured

with hydrogel extracts for 5 d. Following incubation, the cells were treated with staining working solution at room temperature for 30 min and visualized under a fluorescence microscope (Zeiss).

2.13. Scratch assays

NPCs were cultured at a density of 24,000 cells per well in 12-well plates until they reached full confluency. A sterile pipette tip with a volume of 200 μL was utilized to create a straight wound in the cell layer, followed by the replacement of the culture medium with the hydrogel leachate. The migration of NPCs was evaluated by measuring the distance between the two scratched edges at 0, 4, 8, and 16 h after the scratch using Image J software.

2.14. ROS detection

The intracellular levels of ROS were detected using the ROS detection kit (Beyotime). Specifically, cells were incubated with 10 μM 2′,7′-dichlorofluorescein diacetate (DCFH-DA), a fluorescent probe for ROS, at 37 °C for 15 min in the absence of light. Immunofluorescence images were captured using fluorescence microscopy (Zeiss), and the fluorescence intensity was quantified using Image J software.

2.15. Establishment of a rat IVDD model

A total of thirty male SD rats, with an average body weight ranging from 300 to 350 g, were procured from the Experimental Animal Center of Soochow University. The Ethics Committee of Soochow University granted approval for all animal experiments (SUDA20220105A02). After administering anesthesia, a 20 G needle was percutaneously inserted through segments 7–8 (Co7-8) and 8–9 (Co8-9) of the caudal vertebrae to access the NP center. The needle was retained *in situ* for 1 min following each puncture [28]. The rats undergone puncture-induced IVDD were subsequently randomized into four groups, namely, Saline, Hydrogel, KGN (25 mg/mL), and Hydrogel@KGN. Sham-operated rats served as a control. Using a microsyringe (Hamilton, Reno, Nevada, USA), either two microliters of KGN solution or Hydrogel@KGN were injected into NP sites. Following a 4 and 8-week post-surgery period, IVD samples were collected from each group for subsequent experimentation.

2.16. Radiology assessment

X-ray (RADspeed M, Shimadzu, Japan) and magnetic resonance imaging (MRI, GE Signa HDe 1.5T Equipment, General Electric Company, Boston, MA, USA) were conducted on the rat caudal vertebrae, and lateral radiographs were utilized to determine disc height. IVD height index (DHI) was calculated using the following formula: DHI% = Determination of DHI points at each time point in DHI/NC group × 100%. The water content of the IVD was calculated by analyzing the gray value of sagittal T2W1 MRI disc, in accordance with the following parameters: TR = 3500 ms, TE = 102 ms and section thickness = 1.4 mm. The MRI images were categorized into grade I to V based on the improved Thomson classification and Pfirrmann grade [29].

2.17. Histological and immunohistochemical analysis

Four and eight weeks after the surgery, IVD specimens were harvested, fixed in 10% formalin (Sigma–Aldrich) for 48 h, decalcified in 10% ethylene diamine tetraacetic acid (EDTA) for 60 d, and subsequently embedded in paraffin. The specimens were sectioned into 6-μm slices and subjected to staining with safranin O and fast green (S.O., Sigma–Aldrich) or hematoxylin and eosin (H&E, Sigma–Aldrich). Tissue images were captured using a bright field microscope (Zeiss) and histological scores were calculated independently by two independent observers (Y.L. and X.T.) [30].

For immunohistochemical staining, the sections were hydrated with xylene, deparaffinized using graded alcohol, and treated with 3% H_2O_2 (Sigma–Aldrich) for 15 min. Subsequently, the slides were subjected to incubation with primary antibodies including anti-COLII (ab34712, Abcam), anti-ACAN (A11691, Abclonal), anti-IL-1β (16806-1-AP, Proteintech, Rosemont, IL, USA), and anti-NRF2 (A21176, Abclonal), followed by treatment with biotin-labeled secondary antibody at 37 °C for 30 min. Subsequent to this, the slides were stained with 3,3′-diaminobenzidine solution (DAB, Cell Signaling Technology, Danvers, MA, USA) and nuclear counterstaining was performed using hematoxylin (Sigma–Aldrich). The resultant staining images were captured using a bright field microscope (Zeiss) and semi-quantitative analysis was carried out using Image J software.

2.18. Statistical analysis

The data were presented as mean ± standard deviation and analyzed using Prism GraphPad 9.3 software (GraphPad Software, San Diego, CA, USA). The unpaired two-tailed Student's *t*-test was employed to compare the two groups, while differences between multiple groups were analyzed employing one-way analysis of variance (ANOVA) with Tukey's post hoc test. P values < 0.05 (* or #) or < 0.01 (** or ##) were considered statistically significant.

3. Results

3.1. KGN promoted ECM anabolism in NPCs under normal culture conditions

To investigate the impact of KGN on cell viability and ECM metabolism, NPCs were exposed to varying concentrations of KGN, ranging from 0.01 to 1 μM. Results from CCK-8 assays revealed that KGN did not elicit any discernible effects on NPC proliferation under normal culture conditions (Fig. 1A). The results of RT-PCR experiments revealed that treatment with KGN led to a significant up-regulation of *Col2a1* mRNA levels, with increases of 2.1-fold at 0.1 μM and 2.6-fold at 1 μM. Additionally, treatment with 1 μM KGN resulted in a 1.5-fold increase in *Acan* transcript levels and a 3.2-fold increase in *Sox9* transcript levels in NPCs (Fig. 1B). Immunofluorescence staining intensity did not show any significant differences in COL II expression (Fig. 1C, Fig. S1B), but a 91.5% increase in ACAN expression was observed in the KGN-treated group compared to the control group (Fig. S1A&C). Furthermore, Western blot analysis demonstrated that treatment with 1 μM KGN resulted in the highest levels of ACAN and SOX9 protein expression, which were 89.8% and 2.7-fold higher than the CTRL group, respectively (Fig. 1D and E).

3.2. KGN protected the ECM metabolic equilibrium in IL-1β-stimulated NPCs

In order to investigate the protective function of KGN in an inflammatory environment, NPCs were subjected to varying concentrations of KGN in the presence of IL-1β. RT-PCR analysis demonstrated that KGN exhibited a dose-dependent effect on the ability of NPCs to produce ECM, even when exposed to IL-1β (Fig. 2A). Additionally, KGN significantly inhibited the expression of matrix-degrading enzymes in IL-1β-stimulated NPCs. Specifically, treatment with 1 μM KGN significantly down-regulated the gene expression of *Mmp13* and *Adamts5* by 70.7% and 72.5%, respectively, compared with the IL-1β group (Fig. 2B). The results of immunofluorescence experiments demonstrated that KGN effectively reversed the inhibitory effects of IL-1β on COL II secretion in NPCs, with a significant increase of 67.2% at 0.01 μM, 1.9-fold at 0.1 μM, and 2.9-fold at 1 μM (Fig. 2C, Fig. S2B). Moreover, the treatment with KGN led to an improvement in the expression level of ACAN (Fig. S2A&C). Western blot analysis further confirmed that KGN played a crucial role in regulating the metabolic balance of the ECM by promoting the expression of

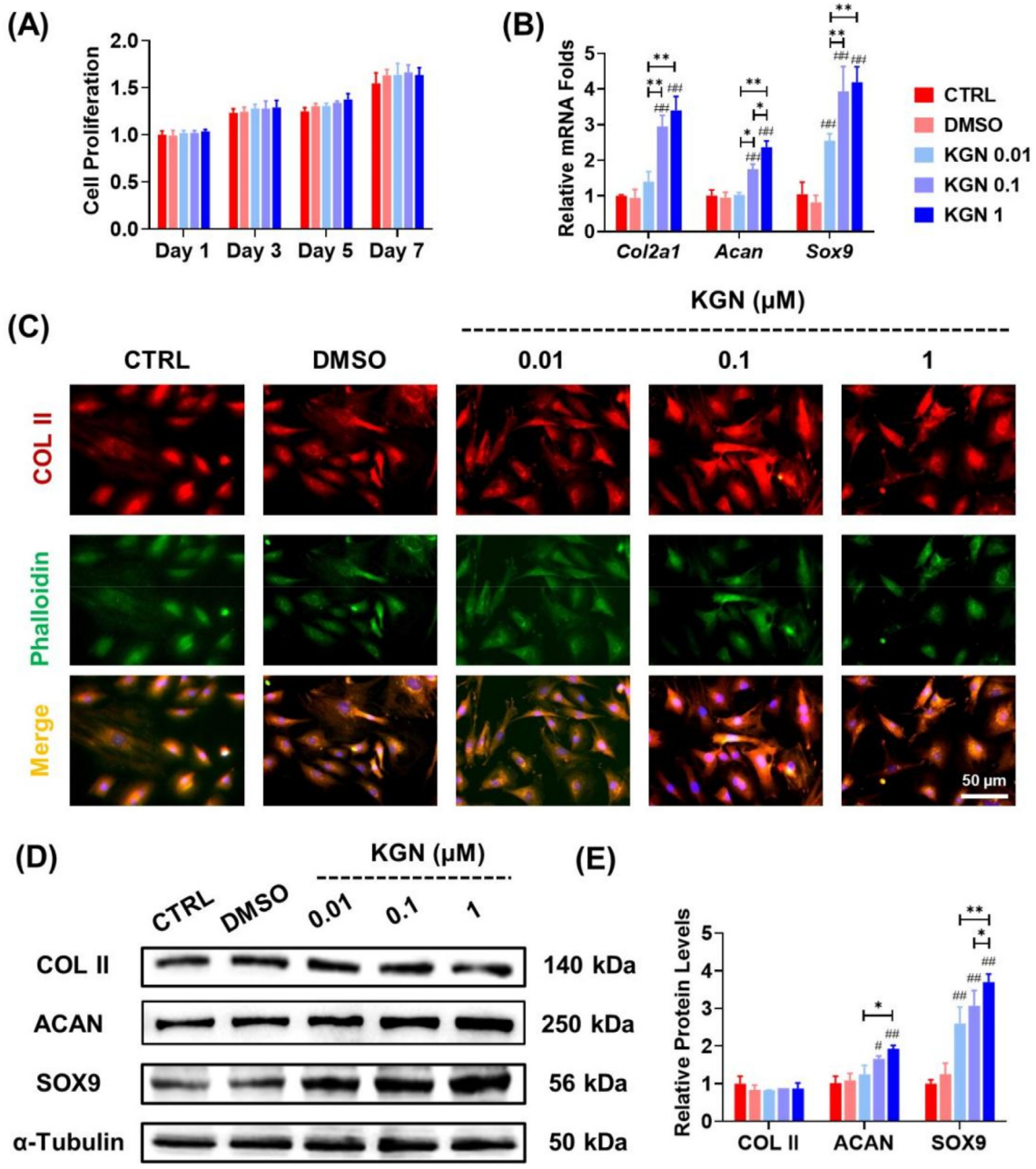

Fig. 1. The effects of KGN on the matrix synthesis of nucleus pulposus cells (NPCs) under normal culture conditions. NPCs were treated with KGN at concentrations of 0.01, 0.1, and 1 μM. (A) Cell proliferation was examined at 1, 3, 5 and 7 days using CCK-8 assay, n = 6. (B) The mRNA expression levels of *Col2a1*, *Acan*, and *Sox9* as determined by RT-PCR, n = 4. (C) Immunofluorescence staining images showed the expression of COL II proteins in KGN-treated cells. (D–E) The effects of KGN on the protein levels of NP matrix components in NPCs were determined using Western blot, n = 3. Data are shown as the mean ± standard deviation. Statistically significant differences are indicated by # where $P < 0.05$ or ## where $P < 0.01$ compared to the control (CTRL) group; * where $P < 0.05$ or ** where $P < 0.01$ between the indicated groups.

anabolic matrix proteins and suppressing the activities of catabolic enzymes (Fig. 2D–F).

3.3. KGN attenuated oxidative stress by enhancing intracellular antioxidant functions in NPCs

In order to unravel the specific mechanisms that underlie the protective effects of KGN on NP matrix metabolism, we conducted an assessment of the intracellular redox status and the integrity of the antioxidant system in NPCs. Our findings indicate that treatment with KGN significantly mitigated intracellular oxidative stress in IL-1β-stimulated NPCs (Fig. 3A, Fig. S3A). Additionally, we observed a 3.8-fold increase in the transcript level of the oxidative regulator *Nrf2* following treatment with 1 μM KGN (Fig. 3B). Furthermore, the mRNA levels of the antioxidant enzymes *Gpx1* (Fig. 3C) and *Hmox1* (Fig. 3D) were increased by 1.2-fold and 5.0-fold, respectively. Western blot assays confirmed the beneficial effects of KGN on the protein expression of these intracellular antioxidant enzymes (Fig. 3E and F).

3.4. Inhibition of NRF2 abrogated KGN-induced protection of ECM in NP

In order to elucidate the role of NRF2 in the regulation of KGN-induced antioxidant functions, NPCs were administered an NRF2-specific inhibitor, ML385, prior to KGN treatment. The

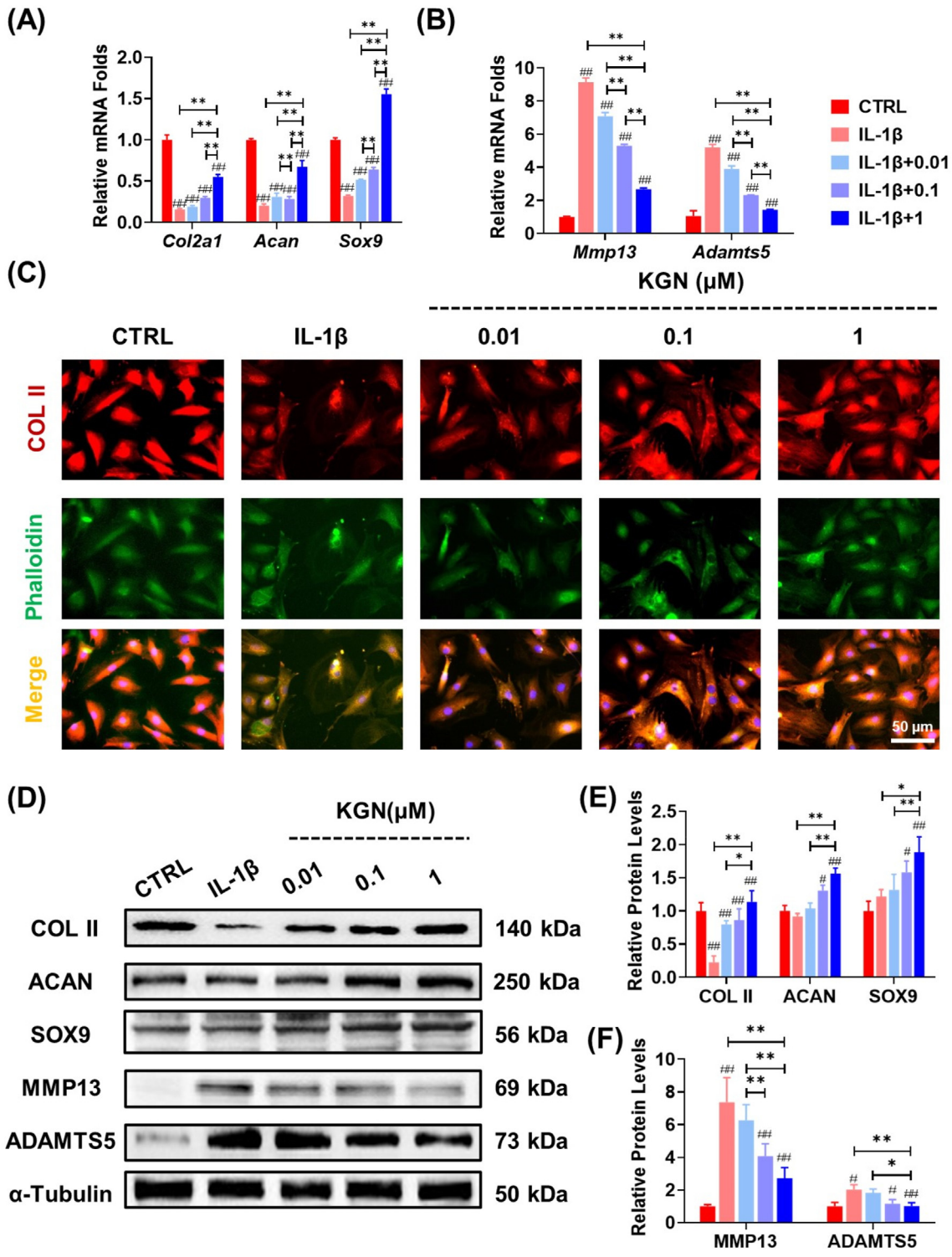

Fig. 2. The protective effects of KGN on ECM metabolism of NPCs in the presence of IL-1β. NPCs were exposed to 5 ng/mL IL-1β and treated with KGN at concentrations of 0.01, 0.1, and 1 μM. (A–B) The mRNA expression levels of *Col2a1*, *Acan*, *Sox9, Mmp13,* and *Adamts5* in IL-1β-treated NPCs were evaluated to assess the effect of KGN, n = 4. (C) Immunofluorescence staining was performed to assess the expression of COL II in NPCs, n = 3. (D–F) The effects of KGN on the protein levels of anabolic or catabolic markers in IL-1β-stimulated NPCs were determined using Western blot, n = 3. Data are presented as the mean ± standard deviation. Statistically significant differences are indicated by # where $P < 0.05$ or ## where $P < 0.01$ compared to the control (CTRL) group; * where $P < 0.05$ or ** where $P < 0.01$ between the indicated groups.

pharmacological inhibition of NRF2 resulted in the elimination of KGN-mediated ROS scavenging effects in IL-1β-stimulated NPCs (Fig. 4A, Fig. S3B). The expression levels of intracellular antioxidant enzymes in KGN-treated NPCs were suppressed following exposure to ML385, both at the transcript and protein levels (Fig. 4B&C). Additionally, the equilibrium of ECM was found to be dysregulated in ML385-treated NPCs, as evidenced by the down-regulation of *Col2a1*, *Acan*, and *Sox9*, and the up-regulation of *Mmp13* and *Adamts5* mRNA expression levels (Fig. 4D&E).

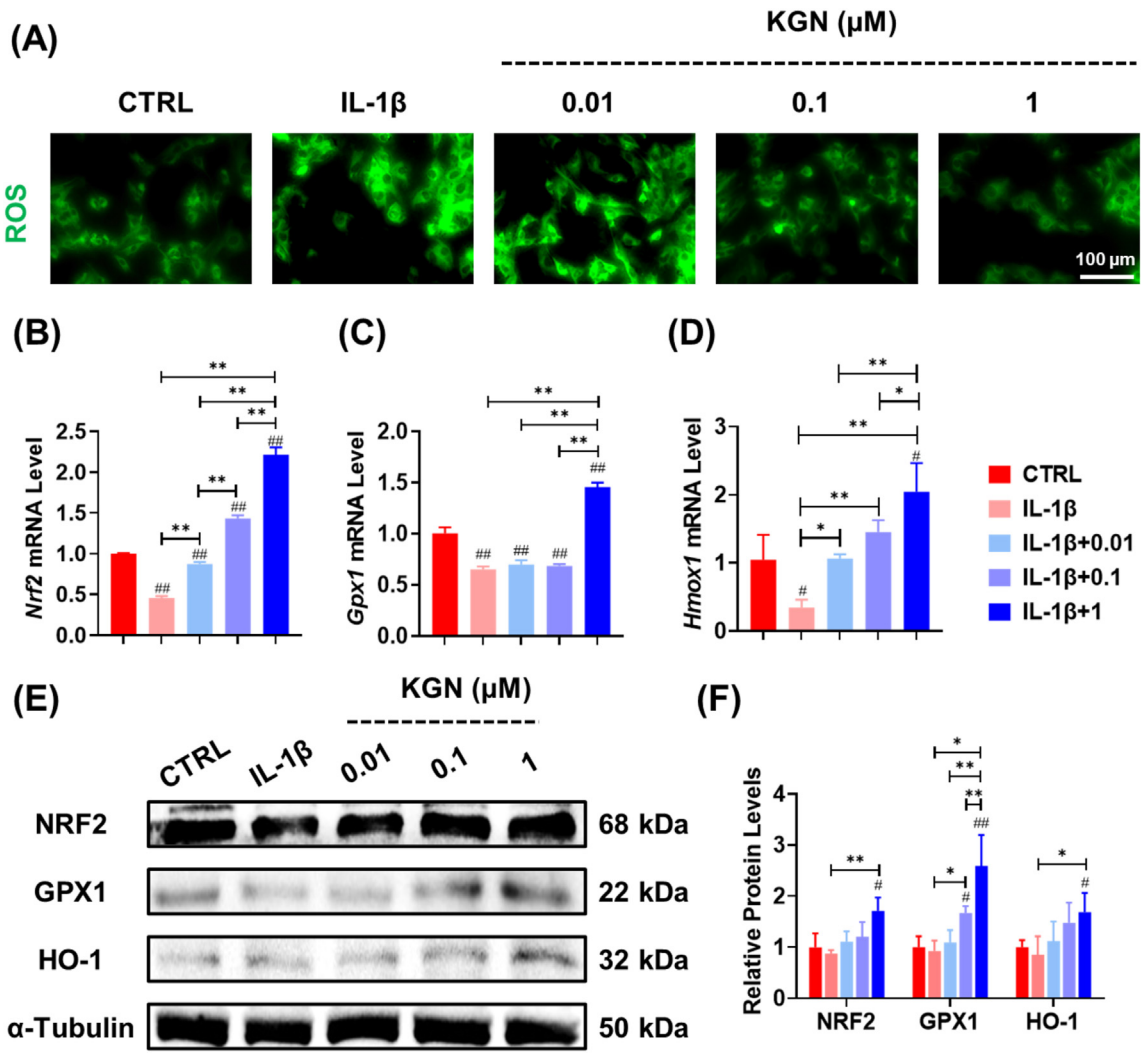

Fig. 3. Impact of KGN on oxidative stress of IL-1β-stimulated NPCs. (A) Immunofluorescence staining indicated the effect of KGN on intracellular ROS in IL-1β-stimulated cells. (B–D) The gene expression of *Nrf2*, *Gpx1*, and *Hmox1* was quantified using RT-PCR, n = 4. (E–F) The effects of KGN on the protein levels of antioxidant enzymes in IL-1β-stimulated NPCs, n = 3. Data are presented as the mean ± standard deviation. Statistically significant differences are indicated by # where $P < 0.05$ or ## where $P < 0.01$ compared to the control (CTRL) group; * where $P < 0.05$ or ** where $P < 0.01$ between the indicated groups.

Western blot assays confirmed that inhibition of NRF2 impeded the protective effects of KGN on the ECM metabolism of NPCs (Fig. 4F, Figs. S4A–C).

3.5. Characterization and biocompatibility of self-healing hydrogel loaded with KGN

The SEM images demonstrate that the Au-Gel hydrogel exhibited a characteristic porous structure with interconnected networks (Fig. 5A), facilitating a controlled and sustained release of KGN (Fig. S5A). Upon the addition of gold ions, the two gelatin chains underwent crosslinking via S–Au–S chemical bonding, resulting in the formation of a reticulated hydrogel (Fig. 5B). The injectable hydrogel was easily administered via a 22 G needle and could be suspended in the air or molded into two complete hydrogel letters (Fig. 5C&D). The hydrogel displayed self-healing properties, as evidenced by its ability to fuse and heal completely within 1 h following complete severance (Fig. 5E). The rheology analysis provided additional evidence that the values of G′ and G″ remained constant within the range of shear frequency from 1 to 50 rad/s (Fig. 5F) or strain range of 0.01–100% (Fig. 5G). Furthermore, cyclic strain tests demonstrated that the values of G′ and G″ recovered after multiple cycles, indicating a stable and dynamic phenomenon (Fig. 5H). The hydrogel's shear viscosity was assessed across a range of shear rates from 0.1 to 50 rad/s, revealing that the dynamic hydrogel exhibited a shear-thinning behavior that could enhance its injectability (Fig. 5I).

Under light microscopy, the morphology of NPCs remained unaltered when cultured with hydrogel or hydrogel@KGN extracts (Fig. 6A). Biocompatibility of the hydrogel was confirmed through Live/dead assays and cell proliferation tests (Fig. 6B–D). The scratch experiment revealed a significantly narrowed scratch width in the hydrogel@KGN group, indicating stronger migration ability during the early stages (Fig. 6E&F).

3.6. In situ injection of Hydrogel@KGN mitigated IVDD progression

To evaluate the therapeutic effects on a puncture-induced rat IVDD model, KGN-laden hydrogel was injected *in situ* for *in vivo* application. The X-ray images demonstrated an improvement in the intervertebral space subsequent to the injection of hydrogel@KGN, as evidenced by an up-regulation of the DHI value by 33.3% and 65.6%, respectively, at 4 and 8 weeks post-surgery, compared to the Saline group (Fig. 7A&C). Similarly, MRI images revealed a restoration of the hydration grade by 36.4% at 4 weeks post-surgery and by 34.8% at 8 weeks post-surgery in

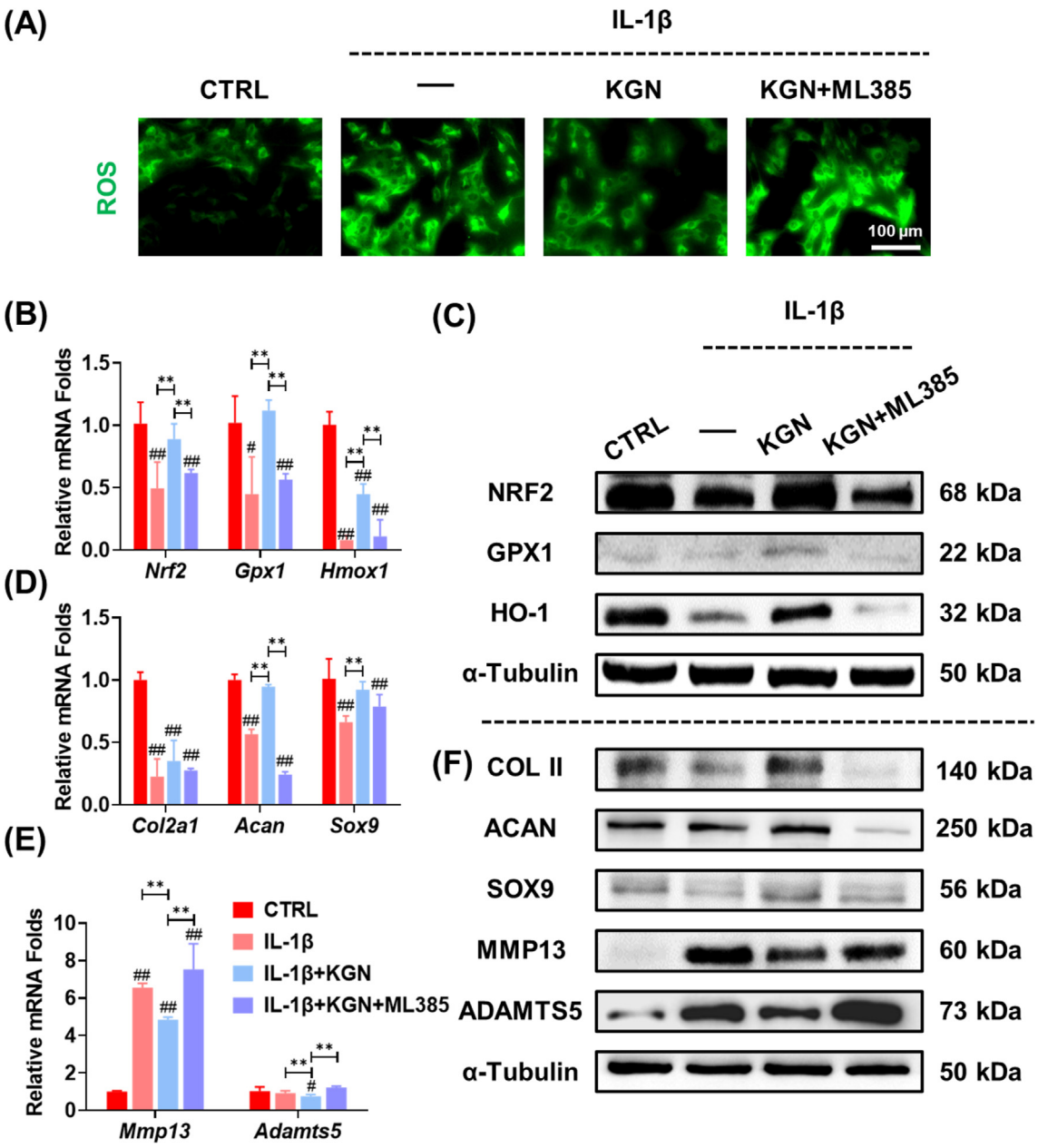

Fig. 4. The role of NRF2 in KGN-modulated antioxidant functions in IL-1β-stimulated NPCs. Prior to exposure to 5 ng/mL IL-1β and 1 μM KGN, NPCs were pre-treated with an NRF2-specific inhibitor, ML385. (A) Immunofluorescence staining revealed intracellular ROS in NPCs. (B) The gene expression of *Nrf2*, *Gpx1*, and *Hmox1* was quantified using RT-PCR, n = 4. (C) The protein levels of NRF2, GPX1, and HO-1 were measured using Western blot, n = 3. (D–E) The gene expression of *Col2a1*, *Acan*, *Sox9, Mmp13,* and *Adamts5* was quantified using RT-PCR, n = 4. (C) The protein levels of COL II, ACAN, SOX9, MMP13, and ADAMTS5 were measured using Western blot. Data are presented as the mean ± standard deviation. Statistically significant differences are indicated by # where $P < 0.05$ or ## where $P < 0.01$ compared to the control (CTRL) group; * where $P < 0.05$ or ** where $P < 0.01$ between the indicated groups.

rats that received the hydrogel@KGN injection, compared to the Saline group (Fig. 7B&D). Histological staining further confirmed the efficacy of the hydrogel@KGN treatment, as evidenced by improved NP morphology and glycosaminoglycans (GAGs) content (Fig. 8A&B). Quantitative analysis demonstrated that the injection of hydrogel@KGN significantly reduced the histological score and the modified Thompson score by 31.0% (Figs. 8C) and 55.6% (Fig. 8D) at 8 weeks post-surgery, respectively, compared to the Saline group.

The immunohistochemical analysis was conducted to further investigate the therapeutic efficacy of hydrogel@KGN on NP degeneration. The Saline group exhibited a significant reduction in COL II (Fig. 9A) and ACAN (Fig. 9B), which was in line with the findings obtained from S.O. staining. Treatment with KGN alone provided minimal protection to the NP ECM. However, treatment with hydrogel@KGN effectively preserved the deposition of COL II and ACAN, resulting in an 84.4% (Fig. S6A) and 2.4-fold (Fig. S6B) increase, respectively, compared to the Saline group at 8 weeks post-surgery. Furthermore, the hydrogel@KGN group exhibited a robust and extensive NRF2 expression in the NP space (Fig. 9C, Fig. S6C), surpassing that of the Saline group by 108.8% (4 weeks post-surgery) and 101.4% (8 weeks post-surgery). Additionally, the administration of hydrogel@KGN significantly decreased the expression of IL-1β, which was 75.8% (4 weeks post-surgery) and 88.6% (8 weeks post-surgery) lower than that of the Saline group (Fig. 9C, Fig. S6C). These findings suggest that the use of hydrogel@KGN not only preserved the deposition of NP extracellular matrix components, such as COL II and ACAN, but also mitigated inflammation in the degenerative IVD.

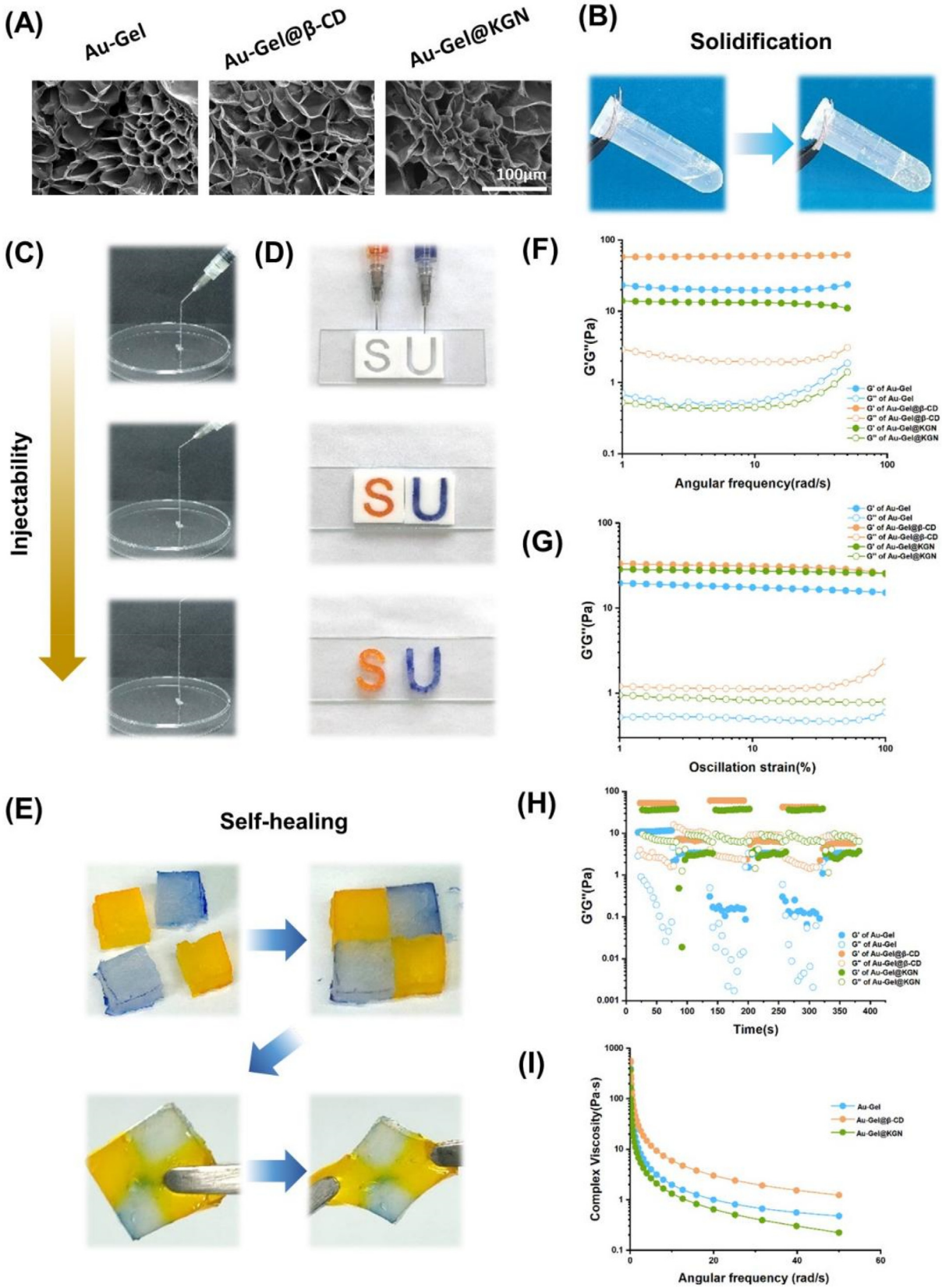

Fig. 5. Characterization of Au-Gel dynamic hydrogel loaded with KGN. (A) Representative SEM images of Au-Gel, Au-Gel@β-CD, and Au-Gel@KGN hydrogels. (B) The gelling process of hydrogel was determined by the inverting experiment. (C–D) The self-healing hydrogel exhibited injectability that can form letter patterns (Soochow university, SU). (E) The self-healing capacity of hydrogel after fragmentation. (F–I) The dynamic oscillatory frequency sweeps (strain = 1%), the strain amplitude sweeps (frequency = 1 rad/s), and the step-strain sweeps (strain = 1 or 300%, frequency = 1 rad/s), the shear viscosity (shear rates ranging from 0.1 to 50 rad/s) of the hydrogel (G′, storage modulus; G″, loss modulus).

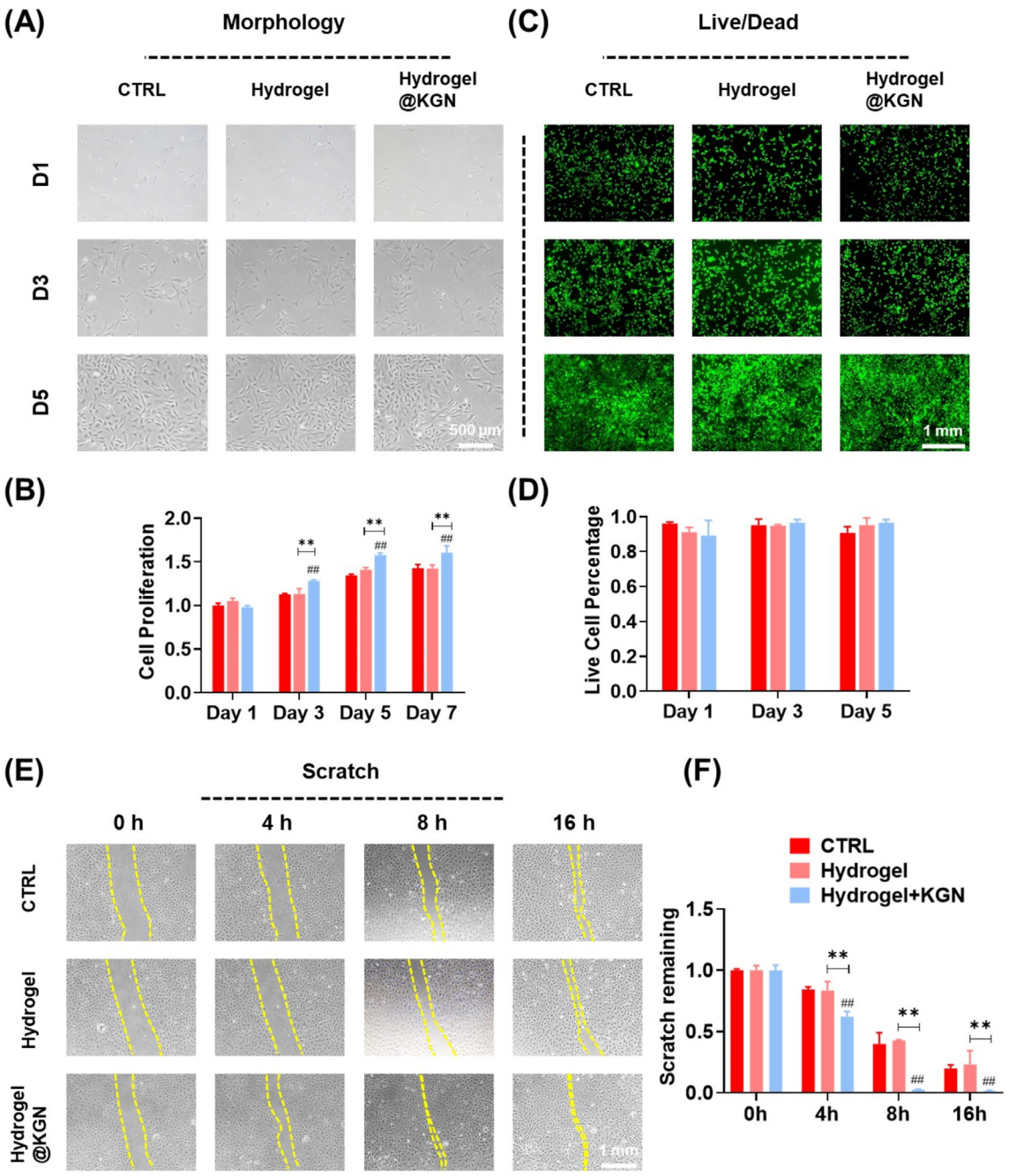

Fig. 6. The biocompatibility of the self-healing Hydrogel@KGN. (A) The cell morphology of NPCs cultured with hydrogel leachate. (B) Cell proliferation of NPCs treated with hydrogel leachate was determined using CCK-8 assays, n = 6. (C) Representative images of Live/dead staining of NPCs treated with hydrogel leachate. (D) Quantification of live and dead cells, n = 3. (E–F) Cell migration at 0, 4, 8, 16 h after cultured with hydrogel leachate, n = 3. Data are presented as the mean ± standard deviation. Statistically significant differences are indicated by # where $P < 0.05$ or ## where $P < 0.01$ compared to the control (CTRL) group; * where $P < 0.05$ or ** where $P < 0.01$ between the indicated groups.

4. Discussion

Given that IVD injury and age-related NP degeneration are irreversible processes, it is imperative to investigate the efficacy of KGN in preventing ECM loss under both normal and degenerative conditions. Our findings indicate that KGN promotes the deposition of anabolic proteins in NPCs cultured under normal conditions, and restores balanced ECM metabolism by re-establishing the equilibrium between anabolism and catabolism in a pro-inflammatory cytokine-induced degenerative environment. The beneficial effects of KGN on ECM components, such as COL I and COL II, have been demonstrated in the context of meniscus degeneration [31] and rotator cuff injury [32]. Li et al. utilized a 3D printing approach to fabricate a poly (ε-caprolactone) (PCL) scaffold that was modified with KGN-loaded poly(lactic-co-glycolic) acid (PLGA) microsphere to augment the secretion of collagen and proteoglycan [33]. However, the precise mechanisms underlying the effects of KGN on cartilaginous matrix homeostasis and its protective role against IVDD remain to be elucidated. It has been proposed that KGN-mediated dissociation of filamin A and CBF-β can enhance chondrogenesis by regulating the transcriptional program of CBF-β-RUNX family transcription factor 1 (RUNX1). The current investigation has demonstrated that the antioxidant properties of KGN, in conjunction with its inherent

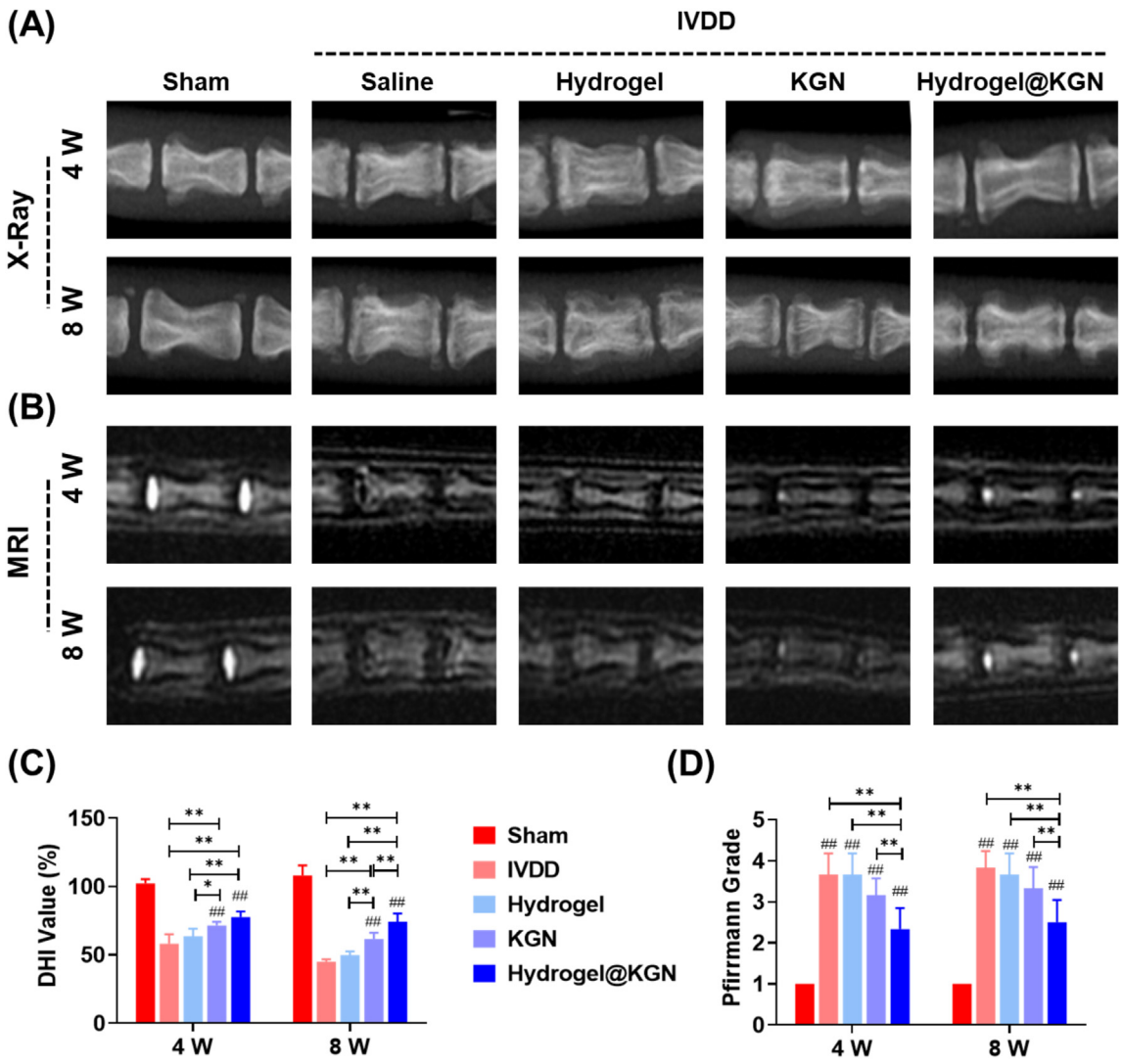

Fig. 7. Diagnostic imaging analyses were conducted to evaluate the impact of Hydrogel@KGN on puncture-induced NP degeneration. A) Representative X-ray images of treated sites in rats' caudal IVDs at 4 and 8 weeks post-surgery. (B) Representative MRI images of treated sites in rats' caudal IVDs 4 and 8 weeks after surgery. (C) The disc height index (DHI) was calculated from the radiograph images, n = 6. (D) The optical density values of IVD based on MRI signals were utilized to indicate the degeneration of rats' caudal IVDs, n = 6. Statistically significant differences are indicated by # where $P < 0.05$ or ## where $P < 0.01$ compared to the Sham group; * where $P < 0.05$ or ** where $P < 0.01$ between the indicated groups.

pro-chondrogenic capacity, exhibit exceptional reparative potential for IVDD. In line with these findings, Yu et al. have encapsulated KGN and apocynin within an injectable esterase-responsive micelle to mitigate cellular apoptosis and enhance autophagy in ADSCs. The *in vivo* application of this cell-encapsulated micelle has been shown to ameliorate disc degeneration [34]. KGN has the potential to function as a molecule that is sensitive to non-coding RNAs, such as miR-146a-5p, miR-145-5p, and miR-381-3p, which can lead to an impact on chondrogenic differentiation or matrix degradation [35,36]. The most commonly observed changes in human degenerated IVDs include a significant reduction in GAGs and the GAG-to-collagen ratio. Yang et al. created a nano-material scaffold to imitate the ECM of native NP. This was achieved through chemical modification of collagen and hyaluronic acid (HA), followed by co-precipitation with GAGs in a controllable manner, resulting in a high GAG/collagen ratio of up to 39.1:1. The biomimetic scaffold was found to enhance cell survival and phenotypic expression of bovine NPCs [37]. Future research will explore the impact of KGN on the matrix metabolism of NPCs with regards to the GAG/collagen ratio.

The potential therapeutic strategy for treating IVDD involves targeting oxidative stress and NRF2-mediated antioxidant functions. Quercetin, an antioxidant and senolytic agent, was found to attenuate cellular senescence in IL-1β-treated NPCs and effectively ameliorate puncture-induced IVDD by activating the NRF2 pathway [38]. Zhou et al. utilized Prussian blue nanoparticles (PBNPs) to stabilize SOD1 from ubiquitination-proteasome degradation, thereby improving the mitochondrial function of H_2O_2-treated NPCs and rescuing ROS-induced NP degeneration [15]. The present study focused on the impact of KGN on NRF2, a crucial regulator of the cellular defense system and essential for IVD growth. Prior research has demonstrated a noteworthy reduction in NRF2 expression in degenerated NPCs, and the knockout of *Nrf2* has been observed to cause more severe disc injury in aging-associated IVDD models compared to wild-type mice [39]. A prior investigation conducted by our laboratory demonstrated that KGN amplifies the osteogenic potential of BMMSCs by stimulating the adenosine 5′-monophosphate-activated protein kinase (AMPK) and silent information regulator type 1 (SIRT1) pathways, which are primarily associated with energy metabolism [40]. Notably, NRF2 activated by sulforaphane safeguards against advanced glycation end-products (AGE)-induced ferroptosis in engineered cardiac tissues or diabetic cardiomyopathy in an AMPK-dependent manner [41]. Consequently, it is imperative to explore

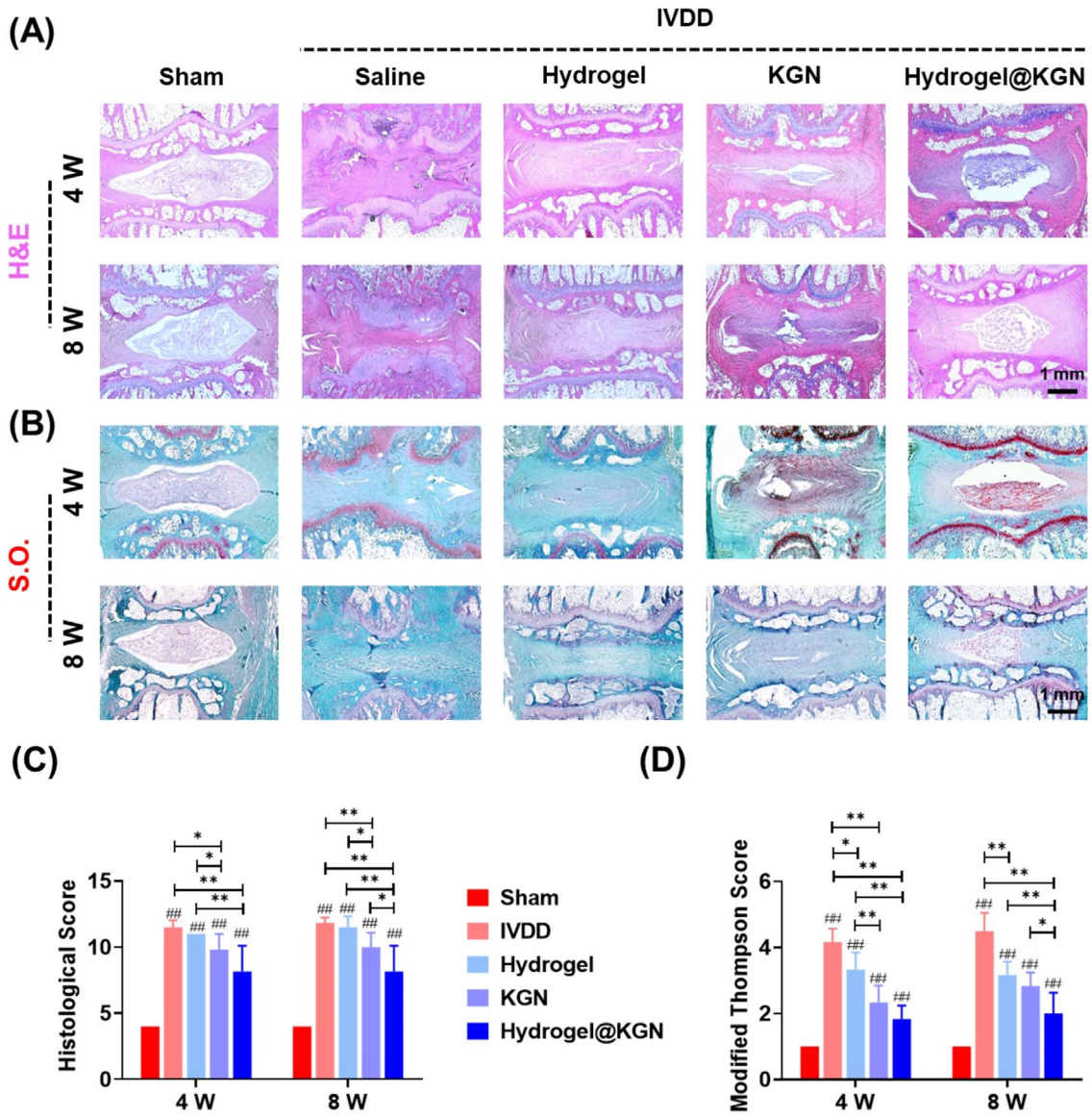

Fig. 8. Histological analysis was conducted to investigate the effect of Hydrogel@KGN on protecting NP matrix in rats' caudal intervertebral discs (IVDs) with puncture injury. (A) Representative images of hematoxylin and eosin (H&E) of IVDs at 4 and 8 weeks post-surgery. Scale bar: 1 mm.(B) Representative images of Safranin O (S.O.) staining of IVDs at 4 and 8 weeks post-surgery. Scale bar: 1 mm. (C–D) Histological scores and the modified Thompson score of the untreated and treated IVDs at 4 and 8 weeks post-surgery, n = 6. Statistically significant differences are indicated by # where $P < 0.05$ or ## where $P < 0.01$ compared to the Sham group; * where $P < 0.05$ or ** where $P < 0.01$ between the indicated groups.

the role of AMPK-SIRT1 in KGN-triggered NRF2 activation in future studies.

The modulation of the local microenvironment involves the inhibition of inflammation, reduction of oxidative stress, and clearance of senescence-associated secretory phenotype, which collectively enhance cell survival and promote tissue regeneration [42]. In this study, we evaluated the redox status by measuring the levels of two critical antioxidant enzymes, GPX1 and HO-1. Our results demonstrate that KGN treatment effectively upregulates the expression of GPX1 and HO-1, thereby mitigating oxidative stress. Mitochondria are known to be a significant source of free radicals generated through oxidative phosphorylation reactions. Recent studies have demonstrated that the use of MSC-derived exosomes for the removal of mitochondrial ROS can effectively mitigate the progression of IVDD [43]. GPX1, a mitochondrion protein, plays a crucial role in reducing mitochondrial ROS by catalyzing the reduction of organic hydroperoxides or H_2O_2 [44]. The knockdown of Gpx1 in chondrogenic cell line ATDC5 has been shown to impair cartilage matrix synthesis, as evidenced by a decrease in the expression of COL II, aggrecan, and SOX9 [45]. Chen et al. have documented that Ginsenoside Rg3, a form of tetracyclic triterpenoid saponin, can prevent NPCs from TNF-α-induced apoptosis and oxidative damage by enhancing the activity of SOD and GPX1 [46]. Conversely, ROS accumulation associated with endoplasmic reticulum (ER) stress has been linked to disc degeneration. A positive correlation has been observed between ER stress and the severity of IVD degeneration in patients with IVDD [47]. HO-1, anchored to the ER, catalyzes the oxidative degradation of cellular heme, resulting in the release of free iron, carbon monoxide (CO), and biliverdin. As a downstream target of NRF2, it plays a crucial role in maintaining redox balance in the ER to mitigate injury to NPCs. The over-expression of HO-1 has been found to protect NPCs homeostasis by alleviating senescence or activating autophagy [48]. Based on these findings, it is possible that KGN induces dual antioxidant effects on both mitochondria and ER, indicating its potential to modulate local redox balance.

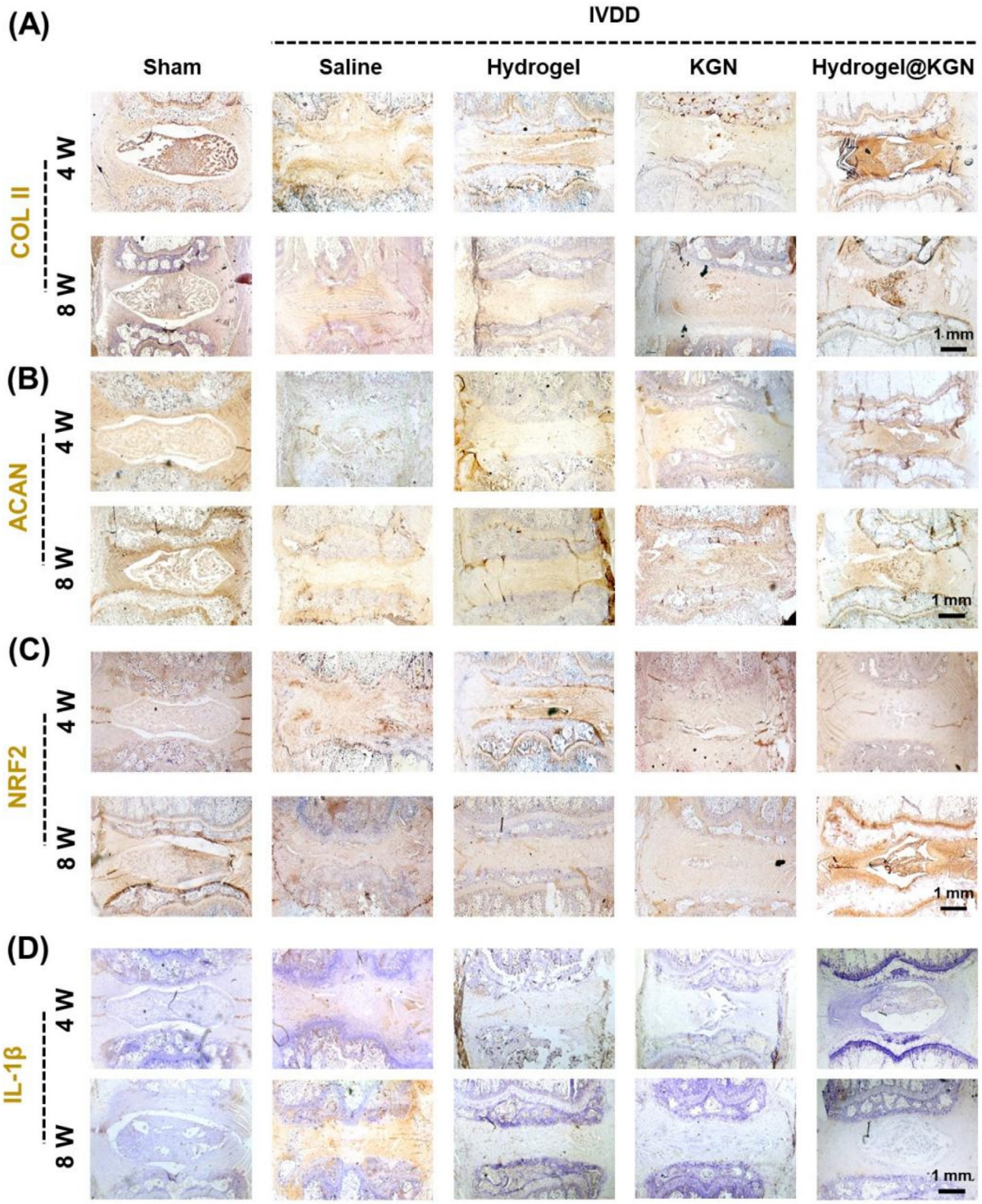

Fig. 9. Immunohistochemical (IHC) analysis was conducted to investigate the NP matrix preservation in rats' caudal intervertebral discs (IVDs) with puncture injury. (A–D) Representative images of IHC staining for collagen II (COL II), aggrecan (ACAN), NRF2, and IL-1β in the NP site at 4 and 8 weeks post-surgery. Scale bar: 1 mm.

The NP tissue is primarily comprised of water and proteoglycan, enabling it to react to diverse biomechanical stimuli, including swelling pressure, compression modulus, permeability, and shear modulus [49]. Hydrogels derived from natural products, such as gelatin [50], alginate [51], and hyaluronic acid [52] are biocompatible, as they do not produce deleterious degradation products or elicit immunological rejection. In the present investigation, a hydrogel composed of gelatin was developed, exhibiting favorable biocompatibility due to its origin as a catabolite from denatured collagen. The gelatin-based hydrogel was designed to mimic the ECM of the IVD [53]. Xu et al. previously reported on the fabrication of a methacrylic acid-modified gelatin (GelMA) hydrogel, which was loaded with growth factors and adipose-derived MSCs for the purpose of maintaining NP tissue integrity and treating IVDD [54]. However, the harsh microenvironment present at the site of injury led to the destruction of the hydrogel structure, resulting in fragmentation. In this study, we have demonstrated that the incorporation of mental coordination-modified hydrogel can confer self-healing properties through dynamic electrovalent interaction. The reversible nature of the

Au–S coordination bond enables the hydrogels to coordinatively self-heal after repeated rupture. Given the high levels of stress experienced by degenerative discs, hydrogels equipped with self-healing capabilities are well-suited for the regeneration of NP. Jia and colleagues synthesized a glycerol cross-linked polyvinyl alcohol (GPG) hydrogel through the formation of multiple hydrogen bonds between glycerol molecules and poly (vinyl alcohol) (PVA) chains. The injectable hydrogel demonstrated viscoelastic properties akin to native NP tissue and exhibited therapeutic effects in models of IVDD involving needle puncture and NP discectomy [28]. Consequently, the design of ECM-mimicking hydrogels for IVDD treatment and NP reconstruction must consider tissue-matched biomechanical properties.

KGN was incorporated into the hydrogel with cyclodextrin encapsuled to achieve a prolonged drug release. The KGN-enhanced dynamic hydrogel demonstrated a reduction in local inflammation at the puncture injury site of the IVD, as indicated by the decreased expression of IL-1β. In an osteoarthritis rat model, the intra-articular administration of KGN effectively mitigated joint pain severity and enhanced articular cartilage repair by elevating the expression of the anti-inflammatory cytokine IL-10 in chondrocytes [55]. Zhang and colleagues have reported that the combination of KGN and platelet-rich plasma (PRP) has a significant impact on reducing the expression of IL-6, TNF-α, and cyclooxygenase-2 (COX-2) in the tendon-bone injury interface by inhibiting the nuclear factor-kappa B (NF-κB) signaling pathway [56]. Nevertheless, additional research is necessary to explore the suppressive effect of KGN on the inflammatory response in degenerated IVD.

A limitation of the present study pertains to the use of rat NPCs rather than human-derived cells. Kamatani et al. have shown that implantation of cartilaginous tissue derived from human induced pluripotent stem cells (iPSCs) effectively restored the structure of NP tissue, thus

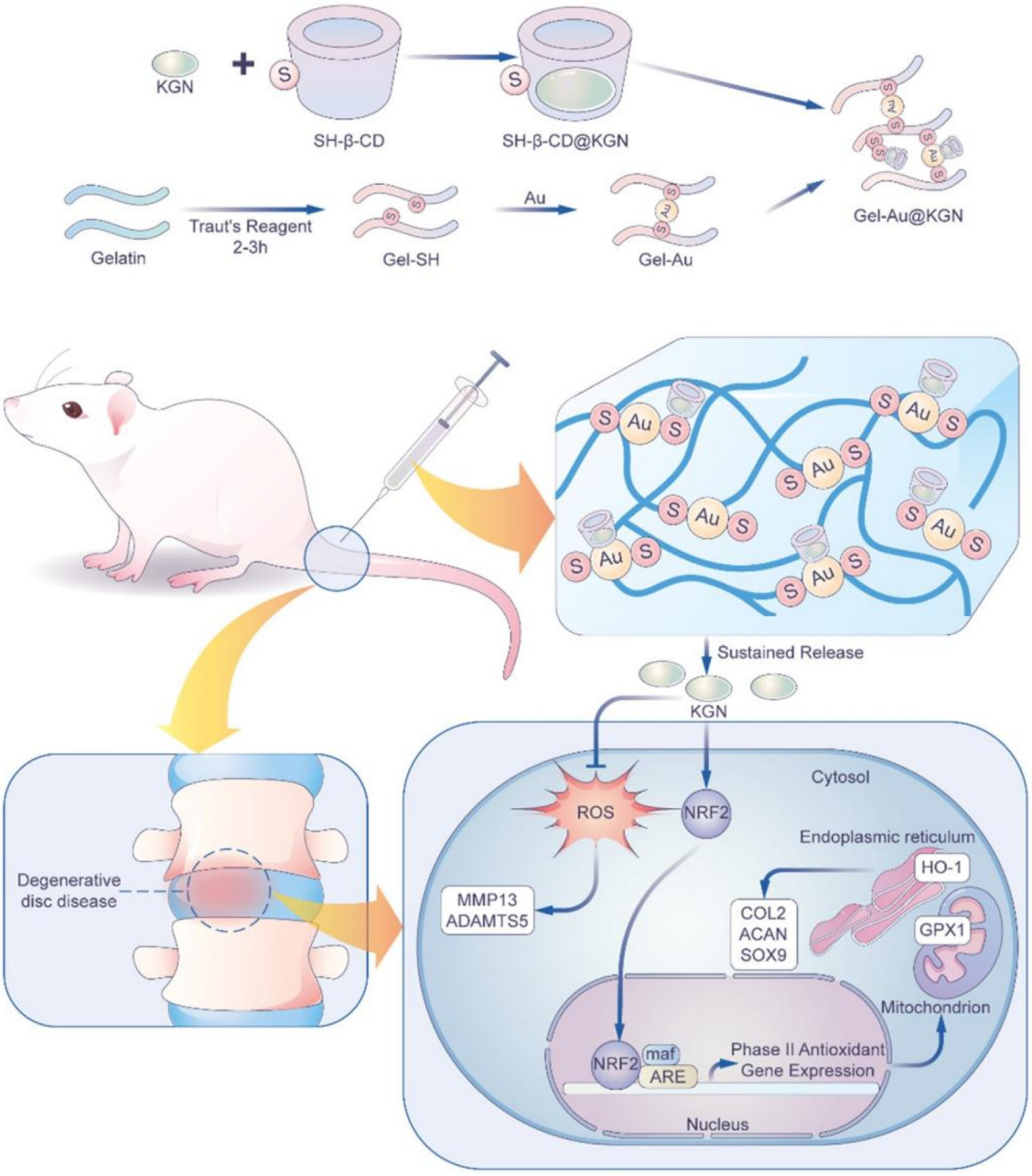

Fig. 10. Kartogenin-enhanced dynamic hydrogel ameliorates IVDD progression. Mechanistically, NRF2 plays an important role in reducing oxidative stress and preventing ECM degradation in NPCs. To achieve localized and sustained release, a self-healing hydrogel loaded with Kartogenin was developed. In situ injection of KGN-enhanced hydrogel mitigates NP degeneration in a rat IVDD model induced by puncture.

indicating its potential as an implant for NP tissue engineering. To facilitate future translation, it is necessary to assess the impact of KGN-enhanced dynamic hydrogel on human primary NPCs or iPSCs [57]. Another limitation was the absence of biomechanical and behavioral analysis. The annulus fibrosus (AF) tissue, in addition to the NP, provides adequate mechanical support to sustain the physiological functions of the IVD [58]. Wei et al. conducted a study in which they incorporated transforming growth factor-β1 (TGF-β1) into polyethylene glycol diacrylate (PEGDA) mixed with decellularized AF matrix. Their findings revealed that the composite hydrogel effectively restored the biomechanical properties of injured IVD by integrating with adjacent AF tissue [59]. Although the antioxidant effects of KGN on AF regeneration remain unclear, the use of ceria-loaded mesoporous silica nanoparticles to mitigate excessive oxidative stress shows potential as a strategy for AF regeneration [60]. Consequently, forthcoming investigations will concentrate on the comprehensive restoration of both NP and AF tissues, ultimately leading to the functional recovery of lumbar IVDs that have undergone herniation.

5. Conclusions

In conclusion, we examined the restorative potential of KGN in NPCs with imbalanced ECM metabolism caused by IL-1β impairment. As illustrated in Fig. 10, the study elucidated the critical role of NRF2 in reducing oxidative stress and preventing ECM degradation in NPCs, as evidenced by the loss of antioxidant and anabolic effects upon pharmacological inhibition of NRF2. Additionally, a self-healing hydrogel loaded with KGN was developed to achieve localized and sustained release of the compound. *In vivo* experiments demonstrated the ability of the KGN-laden hydrogel to mitigate NP degeneration in a rat IVDD model induced by puncture. Collectively, the results of this study indicate that KGN possesses the ability to function as an agent for the regeneration of NP, and that the use of KGN-enhanced dynamic hydrogel may serve as a promising therapeutic intervention for the treatment of IVDD.

Credit authors statement

Xin Tian: Data curation, Formal analysis, Writing - original draft. **Yijian Zhang**: Data curation, Formal analysis, Writing - original draft. **Lei Shen**: Data curation, Formal analysis, Writing - original draft. **Guoqing Pan**: Formal analysis, Methodology, Writing - review & editing. **Huiling Yang**: Supervision, Writing - review & editing. **Zhenhuan Jiang**: Funding acquisition, Investigation, Writing - review & editing. **Xuesong Zhu**: Conceptualization, Funding acquisition, Investigation, Supervision, Writing - review & editing. **Fan He**: Conceptualization, Project administration, Supervision, Formal analysis, Funding acquisition, Writing - original draft, review & editing.

Funding

This work was supported by the Natural Science Foundation of Jiangsu Province (BK20220046); Foundation of Clinical Science and Technology of Wuxi (No. M202172); the Priority Academic Program Development of Jiangsu Higher Education Institutions (PAPD); Jiangsu Health International Exchange Program of Jiangsu Commission of Health (JSH-2018-017); the Postgraduate Research & Practice Innovation Program of Jiangsu Province (KYCX21_2971), Jiangsu Health International Exchange Program of Jiangsu Commission of Health (JSH-2018-017); Medical scientific research project of Jiangsu Provincial Health Commission (Z2020006).

Data availability

The data that support the findings of this study are available from the corresponding author upon reasonable request.

Declaration of competing interest

A conflict of interest occurs when an individual's objectivity is potentially compromised by a desire for financial gain, prominence, professional advancement or a successful outcome. The Editors of the *Journal of Orthopaedic Translation* strive to ensure that what is published in the Journal is as balanced, objective and evidence-based as possible. Since it can be difficult to distinguish between an actual conflict of interest and a perceived conflict of interest, the Journal requires authors to disclose all and any potential conflicts of interest.

Acknowledgement

We want to thanks for Home for Researchers editorial team (www.home-for-researchers.com) for their language editing services.

Appendix A. Supplementary data

Supplementary data to this article can be found online at https://doi.org/10.1016/j.jot.2023.07.002.

References

[1] Mohd Isa IL, Mokhtar SA, Abbah SA, Fauzi MB, Devitt A, Pandit A. Intervertebral disc degeneration: biomaterials and tissue engineering strategies toward precision medicine. Adv. Healthc. Mater. 2022;11:e2102530.
[2] Armbrecht G, Felsenberg D, Ganswindt M, Lunt M, Kaptoge SK, Abendroth K, et al. Degenerative inter-vertebral disc disease osteochondrosis intervertebralis in Europe: prevalence, geographic variation and radiological correlates in men and women aged 50 and over. Rheumatology 2017;56:1189–99.
[3] Berman BM, Langevin HM, Witt CM, Dubner R. Acupuncture for chronic low back pain. N Engl J Med 2010;363:454–61.
[4] Chen S, Wu X, Lai Y, Chen D, Bai X, Liu S, et al. Kindlin-2 inhibits Nlrp3 inflammasome activation in nucleus pulposus to maintain homeostasis of the intervertebral disc. Bone Res 2022;10:5.
[5] Zhou Z, Cui S, Du J, Richards RG, Alini M, Grad S, et al. One strike loading organ culture model to investigate the post-traumatic disc degenerative condition. J. Orthop. Transl. 2020;26:141–50.
[6] Gan Y, He J, Zhu J, Xu Z, Wang Z, Yan J, et al. Spatially defined single-cell transcriptional profiling characterizes diverse chondrocyte subtypes and nucleus pulposus progenitors in human intervertebral discs. Bone Res 2021;9:37.
[7] Zhang C, Smith MP, Zhou GK, Lai A, Hoy RC, Mroz V, et al. Phlpp1 is associated with human intervertebral disc degeneration and its deficiency promotes healing after needle puncture injury in mice. Cell Death Dis 2019;10:754.
[8] Risbud MV, Shapiro IM. Role of cytokines in intervertebral disc degeneration: pain and disc content. Nat Rev Rheumatol 2014;10:44–56.
[9] Kim H, Hong JY, Lee J, Jeon WJ, Ha IH. IL-1β promotes disc degeneration and inflammation through direct injection of intervertebral disc in a rat lumbar disc herniation Model. Spine J 2021;21:1031–41.
[10] Song Y, Li S, Geng W, Luo R, Liu W, Tu J, et al. Sirtuin 3-dependent mitochondrial redox homeostasis protects against AGEs-induced intervertebral disc degeneration. Redox Biol 2018;19:339–53.
[11] Scott JL, Gabrielides C, Davidson RK, Swingler TE, Clark IM, Wallis GA, et al. Superoxide dismutase downregulation in osteoarthritis progression and end-stage disease. Ann Rheum Dis 2010;69:1502–10.
[12] Zheng J, Zhang J, Zhang X, Guo Z, Wu W, Chen Z, et al. Reactive oxygen species mediate low back pain by upregulating substance P in intervertebral disc degeneration. Oxid Med Cell Longev 2021;2021:6681815.
[13] Zhao Y, Qiu C, Wang W, Peng J, Cheng X, Shangguan Y, et al. Cortistatin protects against intervertebral disc degeneration through targeting mitochondrial ROS-dependent NLRP3 inflammasome activation. Theranostics 2020;10:7015–33.
[14] Che H, Li J, Li Y, Ma C, Liu H, Qin J, et al. p16 deficiency attenuates intervertebral disc degeneration by adjusting oxidative stress and nucleus pulposus cell cycle. Elife 2020;9:e52570.
[15] Zhou T, Yang X, Chen Z, Yang Y, Wang X, Cao X, et al. Prussian blue nanoparticles stabilize SOD1 from ubiquitination-proteasome degradation to rescue intervertebral disc degeneration. Adv Sci 2022;9:e2105466.
[16] Johnson K, Zhu S, Tremblay MS, Payette JN, Wang J, Bouchez LC, et al. A stem cell-based approach to cartilage repair. Science 2012;336:717–21.
[17] Cai G, Liu W, He Y, Huang J, Duan L, Xiong J, et al. Recent advances in kartogenin for cartilage regeneration. J Drug Target 2019;27:28–32.
[18] Shi D, Xu X, Ye Y, Song K, Cheng Y, Di J, et al. Photo-cross-linked scaffold with kartogenin-encapsulated nanoparticles for cartilage regeneration. ACS Nano 2016;10:1292–9.
[19] Hou M, Zhang Y, Zhou X, Liu T, Yang H, Chen X, et al. Kartogenin prevents cartilage degradation and alleviates osteoarthritis progression in mice via the miR-146a/NRF2 axis. Cell Death Dis 2021;12:483.

[20] Zhu Y, Tan J, Zhu H, Lin G, Yin F, Wang L, et al. Development of kartogenin-conjugated chitosan-hyaluronic acid hydrogel for nucleus pulposus regeneration. Biomater Sci 2017;5:784–91.
[21] Huang Y, Jiang T, Chen J, Yin GY, Fan J. Effects of kartogenin on the attenuated nucleus pulposus cell degeneration of intervertebral discs induced by interleukin-1β and tumor necrosis factor-α. Int J Mol Med 2018;41:749–56.
[22] Qiao Y, Liu X, Zhou X, Zhang H, Zhang W, Xiao W, et al. Gelatin templated polypeptide Co-Cross-Linked hydrogel for bone regeneration. Adv. Healthc. Mater. 2020;9:e1901239.
[23] Chaudhuri O, Cooper-White J, Janmey PA, Mooney DJ, Shenoy VB. Effects of extracellular matrix viscoelasticity on cellular behaviour. Nature 2020;584:535–46.
[24] Ma Y, He P, Xie W, Zhang Q, Yin W, Pan J, et al. Dynamic colloidal photonic crystal hydrogels with self-recovery and injectability. Research 2021;2021:9565402.
[25] He W, Bai J, Chen X, Suo D, Wang S, Guo Q, et al. Reversible dougong structured receptor-ligand recognition for building dynamic extracellular matrix mimics. Proc Natl Acad Sci U S A 2022;119:e2117221119.
[26] Chen J, Zhu H, Zhu Y, Zhao C, Wang S, Zheng Y, et al. Injectable self-healing hydrogel with siRNA delivery property for sustained STING silencing and enhanced therapy of intervertebral disc degeneration. Bioact Mater 2022;9:29–43.
[27] Peng Y, Qing X, Shu H, Tian S, Yang W, Chen S, et al. Proper animal experimental designs for preclinical research of biomaterials for intervertebral disc regeneration. Biomater. Transl. 2021;2:91–142.
[28] Jia H, Lin X, Wang D, Wang J, Shang Q, He X, et al. Injectable hydrogel with nucleus pulposus-matched viscoelastic property prevents intervertebral disc degeneration. J. Orthop. Translat. 2022;33:162–73.
[29] Pfirrmann CW, Metzdorf A, Zanetti M, Hodler J, Boos N. Magnetic resonance classification of lumbar intervertebral disc degeneration. Spine 2001;26:1873e1878.
[30] Lai A, Gansau J, Gullbrand SE, Crowley J, Cunha C, Dudli S, et al. Development of a standardized histopathology scoring system for intervertebral disc degeneration in rat models: an initiative of the ORS spine section. JOR Spine 2021;4:e1150.
[31] Huang H, Xu H, Zhao J. A novel approach for meniscal regeneration using kartogenin-treated autologous tendon graft. Am J Sports Med 2017;45:3289–97.
[32] Zhu J, Shao J, Chen Y, Zhao G, Li L, Fu Q, et al. Fibrin glue-kartogenin complex promotes the regeneration of the tendon-bone interface in rotator cuff injury. Stem Cells Int 2021;2021:6640424.
[33] Li H, Liao Z, Yang Z, Gao C, Fu L, Li P, et al. 3D printed poly(ε-caprolactone)/meniscus extracellular matrix composite scaffold functionalized with kartogenin-releasing PLGA microspheres for meniscus tissue engineering. Front Bioeng Biotechnol 2021;9:662381.
[34] Yu C, Li D, Wang C, Xia K, Wang J, Zhou X, et al. Injectable kartogenin and apocynin loaded micelle enhances the alleviation of intervertebral disc degeneration by adipose-derived stem cell. Bioact Mater 2021;6:3568–79.
[35] Liu H, Liu P. Kartogenin promotes the BMSCs chondrogenic differentiation in osteoarthritis by down-regulation of miR-145-5p targeting Smad4 pathway. Tissue Eng Regen Med 2021;18:989–1000.
[36] Jing H, Zhang X, Luo K, Luo Q, Yin M, Wang W, et al. miR-381-abundant small extracellular vesicles derived from kartogenin-preconditioned mesenchymal stem cells promote chondrogenesis of MSCs by targeting TAOK1. Biomaterials 2020;231:119682.
[37] Yang XX, Yip CH, Zhao S, Ho YP, Chan BP. A bio-inspired nano-material recapitulating the composition, ultra-structure, and function of the glycosaminoglycan-rich extracellular matrix of nucleus pulposus. Biomaterials 2023;293:121991.
[38] Shao Z, Wang B, Shi Y, Xie C, Huang C, Chen B, et al. Senolytic agent Quercetin ameliorates intervertebral disc degeneration via the Nrf2/NF-κB axis. Osteoarthritis Cartilage 2021;29:413–22.
[39] Tang Z, Hu B, Zang F, Wang J, Zhang X, Chen H. Nrf2 drives oxidative stress-induced autophagy in nucleus pulposus cells via a Keap1/Nrf2/p62 feedback loop to protect intervertebral disc from degeneration. Cell Death Dis 2019;10:510.
[40] Wang Y, Chen G, Yan J, Chen X, He F, Zhu C, et al. Upregulation of SIRT1 by kartogenin enhances antioxidant functions and promotes osteogenesis in human mesenchymal stem cells. Oxid Med Cell Longev 2018:1368142. 2018.
[41] Wang X, Chen X, Zhou W, Men H, Bao T, Sun Y, et al. Ferroptosis is essential for diabetic cardiomyopathy and is prevented by sulforaphane via AMPK/NRF2 pathways. Acta Pharm Sin B 2022;12:708–22.
[42] Chang H, Cai F, Zhang Y, Jiang M, Yang X, Qi J, et al. Silencing gene-engineered injectable hydrogel microsphere for regulation of extracellular matrix metabolism balance. Small Methods 2022;6:e2101201.
[43] Xia C, Zeng Z, Fang B, Tao M, Gu C, Zheng L, et al. Mesenchymal stem cell-derived exosomes ameliorate intervertebral disc degeneration via anti-oxidant and anti-inflammatory effects. Free Radic Biol Med 2019;143:1–15.
[44] Sun Q, Yang Y, Wang Z, Yang X, Gao Y, Zhao Y, et al. PER1 interaction with GPX1 regulates metabolic homeostasis under oxidative stress. Redox Biol 2020;37:101694.
[45] Yan J, Guo Y, Fei Y, Zhang R, Han Y, Lu S. GPx1 knockdown suppresses chondrogenic differentiation of ATDC5 cells through induction of reductive stress. Acta Biochim Biophys Sin 2017;49:110–8.
[46] Chen J, Liu GZ, Sun Q, Zhang F, Liu CY, Yuan L, et al. Protective effects of ginsenoside Rg3 on TNF-α-induced human nucleus pulposus cells through inhibiting NF-κB signaling pathway. Life Sci 2019;216:1–9.
[47] Liao Z, Luo R, Li G, Song Y, Zhan S, Zhao K, et al. Exosomes from mesenchymal stem cells modulate endoplasmic reticulum stress to protect against nucleus pulposus cell death and ameliorate intervertebral disc degeneration in vivo. Theranostics 2019;9:4084–100.
[48] Chen S, Liu S, Zhao L, Lin H, Ma K, Shao Z. Heme oxygenase-1-mediated autophagy protects against oxidative damage in rat nucleus pulposus-derived mesenchymal stem cells. Oxid Med Cell Longev 2020;2020:9349762.
[49] Gao B, Jiang B, Xing W, Xie Z, Luo Z, Zou W. Discovery and application of postnatal nucleus pulposus progenitors essential for intervertebral disc homeostasis and degeneration. Adv Sci 2022;9:e2104888.
[50] Cheng YH, Yang SH, Lin FH. Thermosensitive chitosan-gelatin-glycerol phosphate hydrogel as a controlled release system of ferulic acid for nucleus pulposus regeneration. Biomaterials 2011;32:6953–61.
[51] Tan X, Jain E, Barcellona MN, Morris E, Neal S, Gupta MC, et al. Integrin and syndecan binding peptide-conjugated alginate hydrogel for modulation of nucleus pulposus cell phenotype. Biomaterials 2021;277:121113.
[52] Sloan Jr SR, Wipplinger C, Kirnaz S, Navarro-Ramirez R, Schmidt F, McCloskey D, et al. Combined nucleus pulposus augmentation and annulus fibrosus repair prevents acute intervertebral disc degeneration after discectomy. Sci Transl Med 2020;12:eaay2380.
[53] Bello AB, Kim D, Kim D, Park H, Lee SH. Engineering and functionalization of gelatin biomaterials: from cell culture to medical applications, tissue eng. Part B Rev 2020;26:164–80.
[54] Xu H, Sun M, Wang C, Xia K, Xiao S, Wang Y, et al. GDF5-GelMA injectable microspheres laden with adipose-derived stem cells for disc degeneration repair. Biofabrication 2020;13:015010.
[55] Kwon JY, Lee SH, Na HS, Jung K, Choi J, Cho KH, et al. Kartogenin inhibits pain behavior, chondrocyte inflammation, and attenuates osteoarthritis progression in mice through induction of IL-10. Sci Rep 2018;8:13832.
[56] Zhang L, Zhang Q, Cui L, Wu L, Gao S. Kartogenin combined platelet-rich plasma (PRP) promoted tendon-bone healing for anterior cruciate ligament (ACL) reconstruction by suppressing inflammatory response via targeting AKT/PI3K/NF-κB. Appl Biochem Biotechnol 2023;195:1284–96.
[57] Kamatani T, Hagizawa H, Yarimitsu S, Morioka M, Koyamatsu S, Sugimoto M, et al. Human iPS cell-derived cartilaginous tissue spatially and functionally replaces nucleus pulposus. Biomaterials 2022;284:121491.
[58] Sun H, Wang H, Zhang W, Mao H, Li B. Single-cell RNA sequencing reveals resident progenitor and vascularization-associated cell subpopulations in rat annulus fibrosus. J Orthop Translat 2022;38:256–67.
[59] Wei Q, Liu D, Chu G, Yu Q, Liu Z, Li J, et al. TGF-β1-supplemented decellularized annulus fibrosus matrix hydrogels promote annulus fibrosus repair. Bioact Mater 2022;19:581–93.
[60] Han F, Tu Z, Zhu Z, Liu D, Meng Q, Yu Q, et al. Targeting endogenous reactive oxygen species removal and regulating regenerative microenvironment at annulus fibrosus defects promote tissue repair. ACS Nano 2023;17:7645–61.